

DRK

Technical Report No. 32-677

# Aerodynamic Characteristics of Blunt Bodies

James O. Nichols

Edward A. Nierengarten

FACILITY FORM 502

N65 13301  
(ACCESSION NUMBER)

22  
(PAGES)

W 59914  
(NASA CR OR TMX OR AD NUMBER)

(THRU)

(CODE)

01  
(CATEGORY)

GPO PRICE \$

OTS PRICE(S) \$

Hard copy (HC) 1.00

Microfiche (MF) .50

JET PROPULSION LABORATORY  
CALIFORNIA INSTITUTE OF TECHNOLOGY  
PASADENA, CALIFORNIA

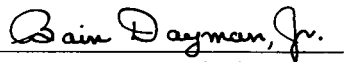
November 19, 1964

*Technical Report No. 32-677*

*Aerodynamic Characteristics of Blunt Bodies*

*James O. Nichols*

*Edward A. Nierengarten*



Bain Dayman, Jr., Chief

Aerodynamic Facilities Section

JET PROPULSION LABORATORY  
CALIFORNIA INSTITUTE OF TECHNOLOGY  
PASADENA, CALIFORNIA

November 19, 1964

Copyright © 1964  
Jet Propulsion Laboratory  
California Institute of Technology

Prepared Under Contract No. NAS 7-100  
National Aeronautics & Space Administration

## CONTENTS

<b>I. Introduction</b> . . . . .	1
<b>II. Summary of Test Results</b> . . . . .	3
A. Normal Force Coefficient Slope $C_{N\alpha}/\text{deg}$ . . . . .	3
1. Round-Shouldered Cylinders . . . . .	3
2. Spherical Segment Models . . . . .	4
3. Spherically Blunted Cones . . . . .	4
B. Center of Pressure at Zero Angle of Attack $X_{cp}/D$ . . . . .	7
1. Round-Shouldered Cylinders . . . . .	7
2. Spherical Segment Models . . . . .	7
3. Blunted Cones . . . . .	8
C. Axial Force Coefficient at Zero Angle of Attack $CA_{\alpha=0}$ . . . . .	10
1. Round-Shouldered Cylinders . . . . .	10
2. Spherical Segment Models . . . . .	10
3. Blunted Cones . . . . .	10
<b>III. Conclusions</b> . . . . .	15
<b>Nomenclature</b> . . . . .	15
<b>References</b> . . . . .	16

## TABLE

<b>1. Average aerodynamic parameters</b> . . . . .	2
--	---

## FIGURES

<b>1. Model configurations: (a) round-shouldered circular cylinders, <math>F = r_c/r_b</math>; (b) spherical segment models, <math>\sigma = T</math>; (c) spherically blunted cones, <math>\sigma = R/r_b</math></b> . . . . .	2
<b>2. Variation of normal force coefficient slope—round-shouldered cylinders: (a) <math>C_{N\alpha}</math> vs. Mach No.; (b) <math>C_{N\alpha}</math> vs. shoulder radius ratio</b> . . . . .	3
<b>3. Variation of normal force coefficient slope—spherical segment models: (a) <math>C_{N\alpha}</math> vs. Mach No.; (b) <math>C_{N\alpha}</math> vs. base angle</b> . . . . .	4
<b>4. Variation of normal force coefficient slope with Mach number—spherically blunted cones: (a) <math>C_{N\alpha}</math> vs. Mach No., <math>R/r_b = 0</math>; (b) <math>C_{N\alpha}</math> vs. Mach No., <math>R/r_b = 0.5</math>; (c) <math>C_{N\alpha}</math> vs. Mach No., <math>R/r_b = 0.75</math>; (d) <math>C_{N\alpha}</math> vs. Mach No., <math>R/r_b = 1.0</math></b> . . . . .	5



## FIGURES (Cont'd)

5. Variation of normal force coefficient slope with bluntness—  
spherically blunted cones: (a)  $C_{N\alpha}$  vs.  $R/r_b$ ,  $M = 1.65$ ;  
(b)  $C_{N\alpha}$  vs.  $R/r_b$ ,  $M = 2.01$ ; (c)  $C_{N\alpha}$  vs.  $R/r_b$ ,  $M = 3.02$  . . . . . 6
6. Variation of center of pressure location—round-shouldered  
cylinders: (a)  $X_{cp}/D$  vs. Mach No.; (b)  $X_{cp}/D$  vs. shoulder  
radius ratio . . . . . 7
7. Variation of center of pressure location—spherical segment  
models: (a)  $X_{cp}/D$  vs. Mach No.; (b)  $X_{cp}/D$  vs. base angle . . . . . 7
8. Variation of center of pressure location at zero angle of attack—  
spherically blunted cones: (a)  $X_{cp}/D$  vs. Mach No.,  $R/r_b = 0$ ;  
(b)  $X_{cp}/D$  vs. Mach No.,  $R/r_b = 0.5$ ; (c)  $X_{cp}/D$  vs. Mach No.,  
 $R/r_b = 0.75$ ; (d)  $X_{cp}/D$  vs. Mach No.,  $R/r_b = 1.0$  . . . . . 8
9. Variation of center of pressure location with bluntness—spherically  
blunted cones: (a)  $X_{cp}/D$  vs.  $R/r_b$ ,  $M = 1.65$ ; (b)  $X_{cp}/D$  vs.  $R/r_b$ ,  
 $M = 2.01$ ; (c)  $X_{cp}/D$  vs.  $R/r_b$ ,  $M = 3.02$  . . . . . 9
10. Variation of axial force coefficient—round-shouldered cylinders:  
(a)  $CA_{\alpha=0}$  vs. Mach No.; (b)  $CA_{\alpha=0}$  vs. shoulder radius ratio . . . . . 10
11. Variation of axial force coefficient—spherical segment models:  
(a)  $CA_{\alpha=0}$  vs. Mach No.; (b)  $CA_{\alpha=0}$  vs. base angle . . . . . 11
12. Variation of axial force coefficient with Mach number—spherically  
blunted cones: (a)  $CA_{\alpha=0}$  vs. Mach No.,  $R/r_b = 0$ ; (b)  $CA_{\alpha=0}$  vs.  
Mach No.,  $R/r_b = 0.5$ ; (c)  $CA_{\alpha=0}$  vs. Mach No.,  $R/r_b = 0.75$ ;  
(d)  $CA_{\alpha=0}$  vs. Mach No.,  $R/r_b = 1.0$  . . . . . 12
13. Variation of axial force coefficient with bluntness—spherically  
blunted cones: (a)  $CA_{\alpha=0}$  vs.  $R/r_b$ ,  $M = 1.65$ ; (b)  $CA_{\alpha=0}$  vs.  $R/r_b$ ,  
 $M = 2.01$ ; (c)  $CA_{\alpha=0}$  vs.  $R/r_b$ ,  $M = 3.02$  . . . . . 13
14. Variation of axial force coefficient with cone half-angle—  
spherically blunted cones: (a)  $CA_{\alpha=0}$  vs.  $\sigma$ ,  $M = 1.65$ ; (b)  $CA_{\alpha=0}$  vs.  
 $\sigma$ ,  $M = 2.01$ ; (c)  $CA_{\alpha=0}$  vs.  $\sigma$ ,  $M = 3.02$  . . . . . 14

## ABSTRACT

13301

The static aerodynamic characteristics of three related families of blunt bodies—spherically blunted cones, spherical segments, and round-shouldered circular cylinders—are presented. Data from tests of blunted cones conducted at the Marshall Space Flight Center and the Wright Air Development Center are presented together with data from tests at JPL to extend the ranges of test parameters. The ranges of parameters are: cone half-angle from 10 to 60 deg; bluntness ratio (nose radius/base radius) from 0 to 1.0; and Mach number from 1.65 to 9.0 with some data at subsonic Mach numbers. The spherical segments and round-shouldered circular cylinders have not been as extensively investigated as the spherically blunted cones. This Report presents the results of the first systematic tests of these bodies.

Test data are compared with sharp cone and modified Newtonian theories.



## I. INTRODUCTION

Because of the interest in various configurations suitable for planetary entry, a survey was made to summarize many of the existing test data on entry configurations. In compiling the summary of entry body characteristics a definite void of practical test information on blunted cones, spherical segments and flat-faced bodies was found. To complete the summary, support existing data on blunted cones, and prepare practical aerodynamic charts with a wide range of parameters, the Jet Propulsion Laboratory (JPL) undertook a program to determine the aerodynamic characteristics of a number of blunt bodies.

The test was conducted in two phases. Phase one was performed in the JPL 20-in. supersonic wind tunnel at Mach numbers 1.65, 2.01, and 3.02, with corresponding Reynolds No./in. of  $0.32 \times 10^6$ . Phase two was performed in the JPL 21-in. hypersonic wind tunnel at Mach No. 5.01

and 9.02, and Reynolds No./in. of  $0.141 \times 10^6$  and  $0.103 \times 10^6$ , respectively. The angle of attack was varied from  $-1$  to  $+20$  deg for phase one and from  $-3$  to  $+19.3$  deg for phase two.

Model configurations (Fig. 1) were comprised of: spherically blunted cones; spherical segments; and flat-faced, round-shouldered, right-circular cylinders. All models had flat bases and no afterbodies. The round-shouldered cylinder models had four ratios of radius of shoulder to base radius: 0.25, 0.50, 0.75, and 1.00. The ratio 1.00 is a hemisphere. The spherical segment models have base angles of 15, 30, 45, and 60 deg as shown. These models represent the bluntest case of the blunted cones with bluntness ratios  $R/r_b$  of 1.035, 1.155, 1.414, and 2.000, respectively. They are also related to the round-shouldered cylinders by the fact that the hemisphere is a member

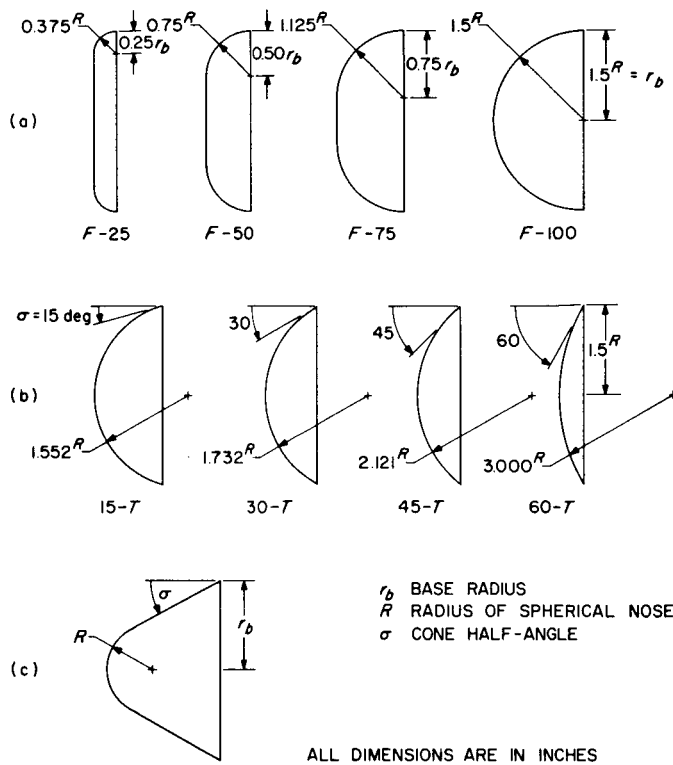


**Fig. 1. Model configurations: (a) round-shouldered circular cylinders,  $F = r_c/r_b$ ; (b) spherical segment models,  $\sigma = T$ ; (c) spherically blunted cones,  $\sigma = R/r_b$**

of this family of bodies. The hemisphere may be considered a spherical segment model with a base angle of 0 deg. The spherically blunted cones have half-angles of 15, 30, 45, and 60 deg and bluntness ratios of 0.25, 0.50, 0.75, and 1.00. The bluntness ratio is defined as the ratio of radius of the spherical nose to the base radius.

In addition to the data for blunted cones obtained in this test, data from Ref. 1 and 2 are presented in order to cover a wide range of Mach numbers, cone angles and bluntness ratios. Reference 1 is a report of data obtained at the Marshall Space Flight Center (MSFC) in the 14-in. transonic and 7-in. supersonic wind tunnels. Spherically blunted cones with half-angles of 10, 13.32, 25, and 50 deg and with bluntness ratios ranging from 0 to 1.244 were tested at Mach 0.5 to 5.0. Reference 2 is a report of data obtained in a test by Convair using the Wright Air Development Center's (WADC) 10-ft. transonic tunnel and JPL's 20-in. supersonic tunnel. Spherically blunted cones with half-angles of 20, 30, and 40 deg and bluntness ratios of 0, 0.4, and 0.6 were tested at Mach 0.5 to 4.06. Table 1 lists the average wind tunnel conditions for these tests.

**Table 1. Average aerodynamic parameters**

Wind tunnel	Mach No.	Reynolds/in. $\times 10^{-6}$	Model dia, in.
JPL 20-in.	1.65	0.317	3
	2.21	0.319	3
	3.02	0.327	3
JPL 21-in.	5.01	0.141	3
	9.02	0.103	3
MSFC 14 by 14 transonic	0.5	0.352	3
	0.7	0.436	3
	0.85	0.489	3
	0.95	0.510	3
	1.15	0.535	3
	1.25	0.535	3
	1.43	0.513	3
MSFC 14 by 14 supersonic	1.93	0.590	3
	2.74	0.402	3
	2.99	0.551	3
	3.48	0.657	3
	4.00	0.717	3
	4.45	0.551	3
	4.96	0.402	3
MSFC 7 by 7 supersonic	1.58	0.350	1.5
	1.99	0.306	1.5
	2.44	0.246	1.5
	2.99	0.187	1.5
	3.26	0.162	1.5
	3.60	0.137	1.5
	3.89	0.117	1.5
Convair WADC 10-ft transonic	4.39	0.094	1.5
	0.85	0.0207	11.25
Convair JPL 20-in. supersonic	1.00	0.0219	11.25
	1.33	0.0246	3
	1.97	0.0206	3
	2.79	0.0146	3
	4.06	0.0072	3

The data presented in this Report include slope of normal force coefficient curve, center of pressure location, and axial force coefficient. The data are shown plotted versus Mach number and in some cases are cross plotted to show the effects of bluntness ratio and of cone half angle. Sharp cone theory (Ref. 3) and modified Newtonian theory are compared with the data. Reference 4 was used to facilitate the Newtonian calculations.

## II. SUMMARY OF TEST RESULTS

### A. Normal Force Coefficient Slope $C_{N\alpha}/\text{deg}$

For most of the models tested the curve of  $C_N$  versus  $\alpha$  is fairly linear over most of the  $\alpha$  range at the test Mach numbers; exceptions are the 30- and 45-deg cones which are practically linear up to about 10 deg of angle of attack. Linearity was found (Ref. 1 and 2) over angle of attack ranges of  $\pm 4$  deg, and for most cases practical linearity over the entire  $\alpha$  range in which maximum  $\alpha$  was 10 and 12 deg, respectively.

### 1. Round-Shouldered Cylinders

Figure 2a is a plot of  $C_{N\alpha}$  versus Mach number and shows little variation of  $C_{N\alpha}$  with Mach number above  $M = 3$ . The data also show that  $C_{N\alpha}$  increases with increasing shoulder radius ratio. Agreement with modified Newtonian theory is good except for the hemisphere  $F-100$ . Figure 2b is a cross plot of the data showing the variation of  $C_{N\alpha}$  with shoulder radius ratio at the lower Mach numbers.

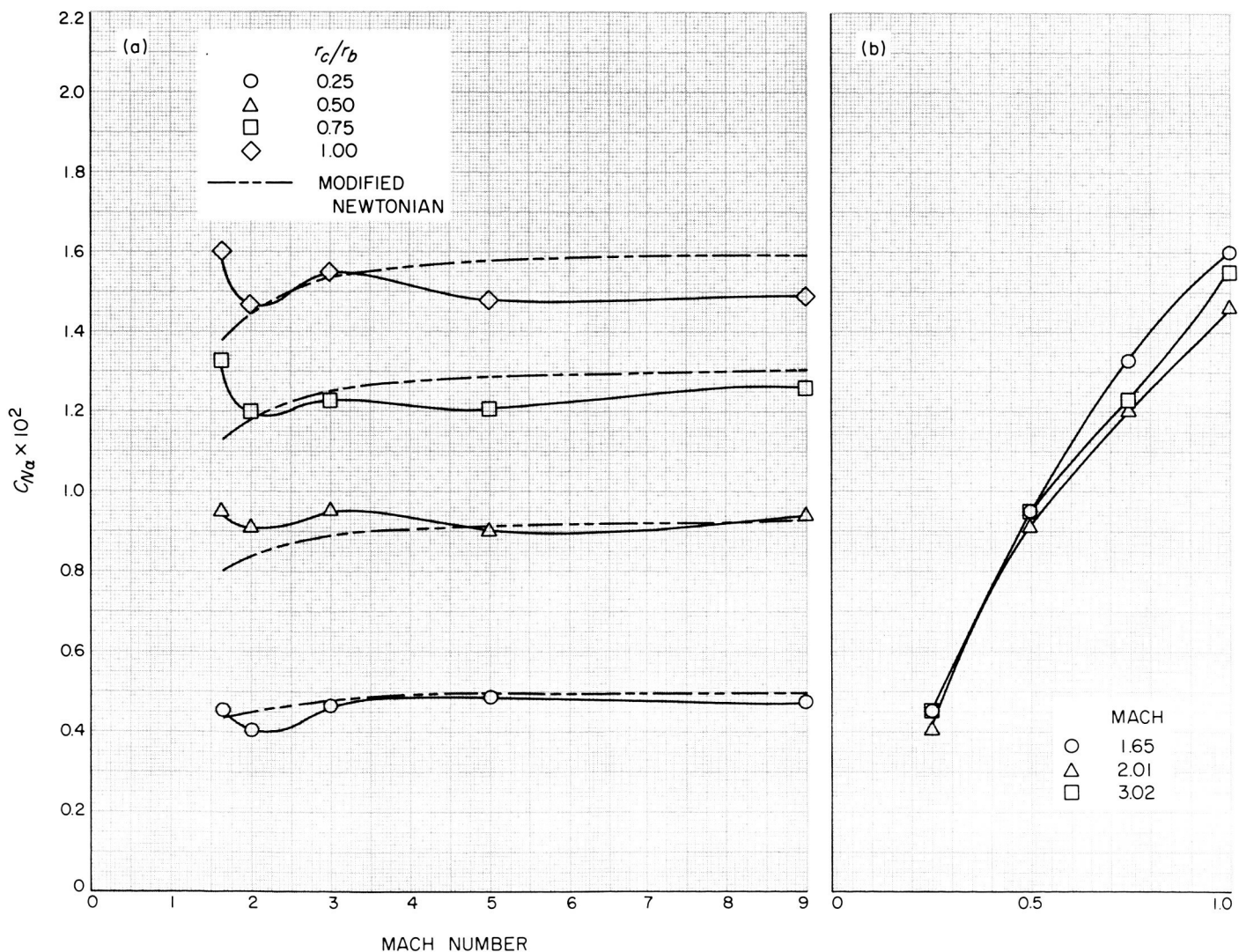


Fig. 2. Variation of normal force coefficient slope—round-shouldered cylinders: (a)  $C_{N\alpha}$  vs. Mach No.; (b)  $C_{N\alpha}$  vs. shoulder radius ratio

## 2. Spherical Segment Models

Figure 3a shows the variation of  $C_{N\alpha}$  with Mach number. There is little variation with Mach number above  $M = 3$ ; however, the data show that except for the hemisphere  $F = 100$  there is a continual increase in  $C_{N\alpha}$  with Mach number. Modified Newtonian theory predicts values somewhat higher than experimental data. Figure 3b is a cross plot showing the effect of  $\sigma$  on  $C_{N\alpha}$ .

## 3. Spherically Blunted Cones

Figure 4 shows the variation of  $C_{N\alpha}$  with Mach number for blunted cones of various bluntness ratios. The data for bluntness ratio  $R/r_b = 0$  shown in Fig. 4a are taken from Ref. 1 and 2 and are compared with pointed cone theory from Ref. 3 and modified Newtonian theory.

The data are in good agreement with the theory of Ref. 3 at Mach numbers above shock attachment where the theory is applicable. Modified Newtonian theory slightly underestimates  $C_{N\alpha}$ . Figure 4b shows interpolated data from Ref. 1 and 2 compared with the present data for a bluntness ratio of 0.5. Interpolation was necessary because of the bluntness ratios used in Ref. 1 and 2. Data for bluntness ratios of 0.75 and 1.00 are shown in Fig. 4c and 4d, respectively. The plots show that Mach number effect on  $C_{N\alpha}$  is small above  $M = 3$  except for the 50-deg cone. For clarity the Newtonian values are shown for  $M = 5$  only.

Figure 5 is a cross plot of  $C_{N\alpha}$  to show variation with bluntness ratio. At the lower Mach numbers, 1.65 and 2.01, bluntness has little effect on  $C_{N\alpha}$  up to a bluntness

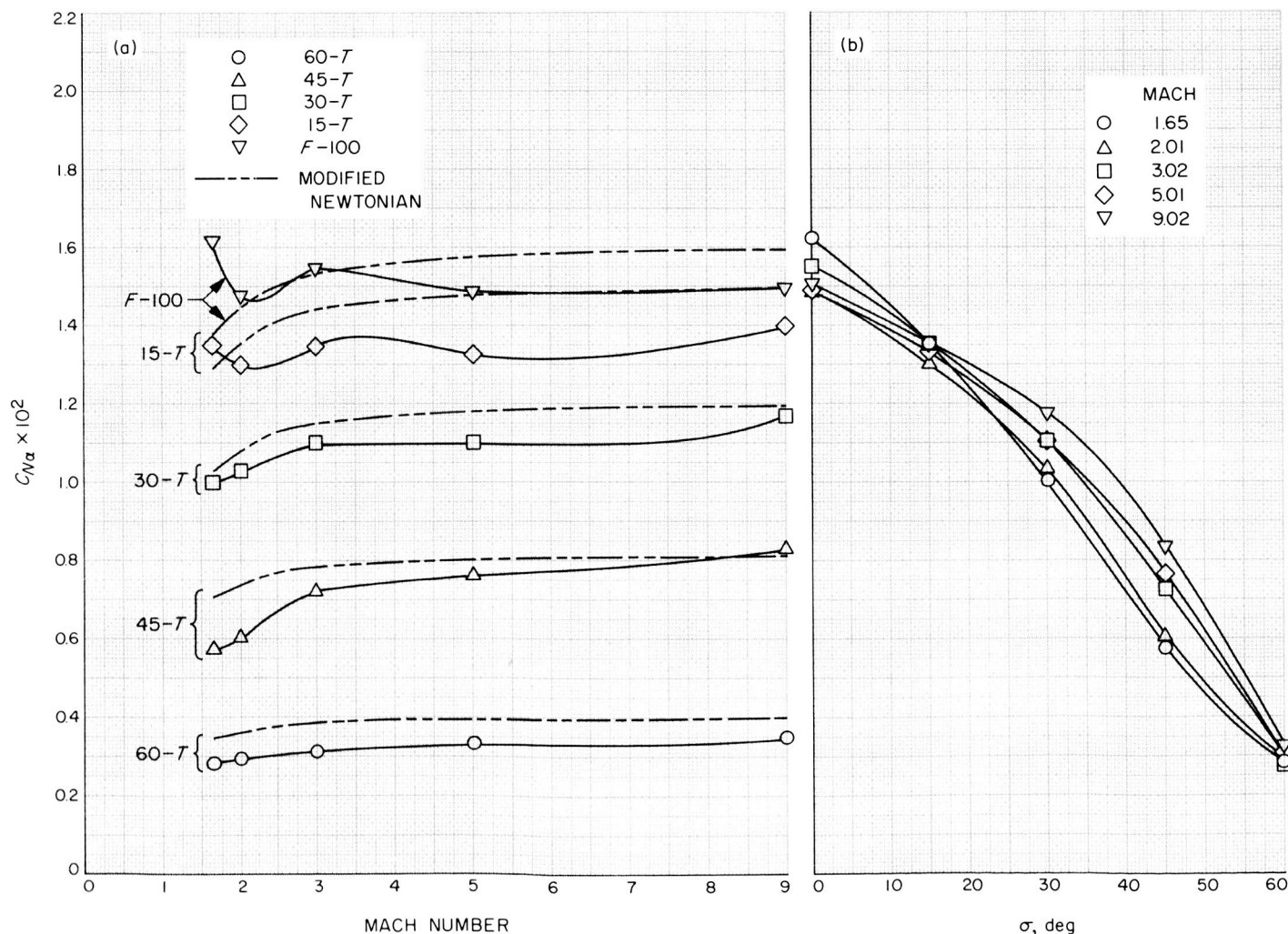


Fig. 3. Variation of normal force coefficient slope—spherical segment models: (a)  $C_{N\alpha}$  vs. Mach No.; (b)  $C_{N\alpha}$  vs. base angle

ratio of about 0.5. Above this bluntness ratio the cones with small half-angles tend toward a uniform value of  $C_{N\alpha}$  of about 0.014 to 0.018 at  $R/r_b = 1.0$ . The Mach number at which the data converge depends on the cone half-angle, as shown in Fig. 4d. At  $M = 2$  the 20- and 30-deg cone data have merged while the 45-deg cone data converge about  $M = 5$ . The 60-deg cone data do not converge. Both 50- and 60-deg cones appear to be essentially unaffected by bluntness.

Considerable interpolation was necessary in plotting Fig. 5 since it represents a compilation of data from three sources. To interpolate between Mach numbers, the data were read directly from plots of  $C_{N\alpha}$  versus Mach number presented in the references. Plots of  $C_{N\alpha}$  versus cone angle with constant bluntness ratio and Mach number were used to interpolate the data for extending the range of bluntness ratio to show a variation of normal force coefficient with bluntness.

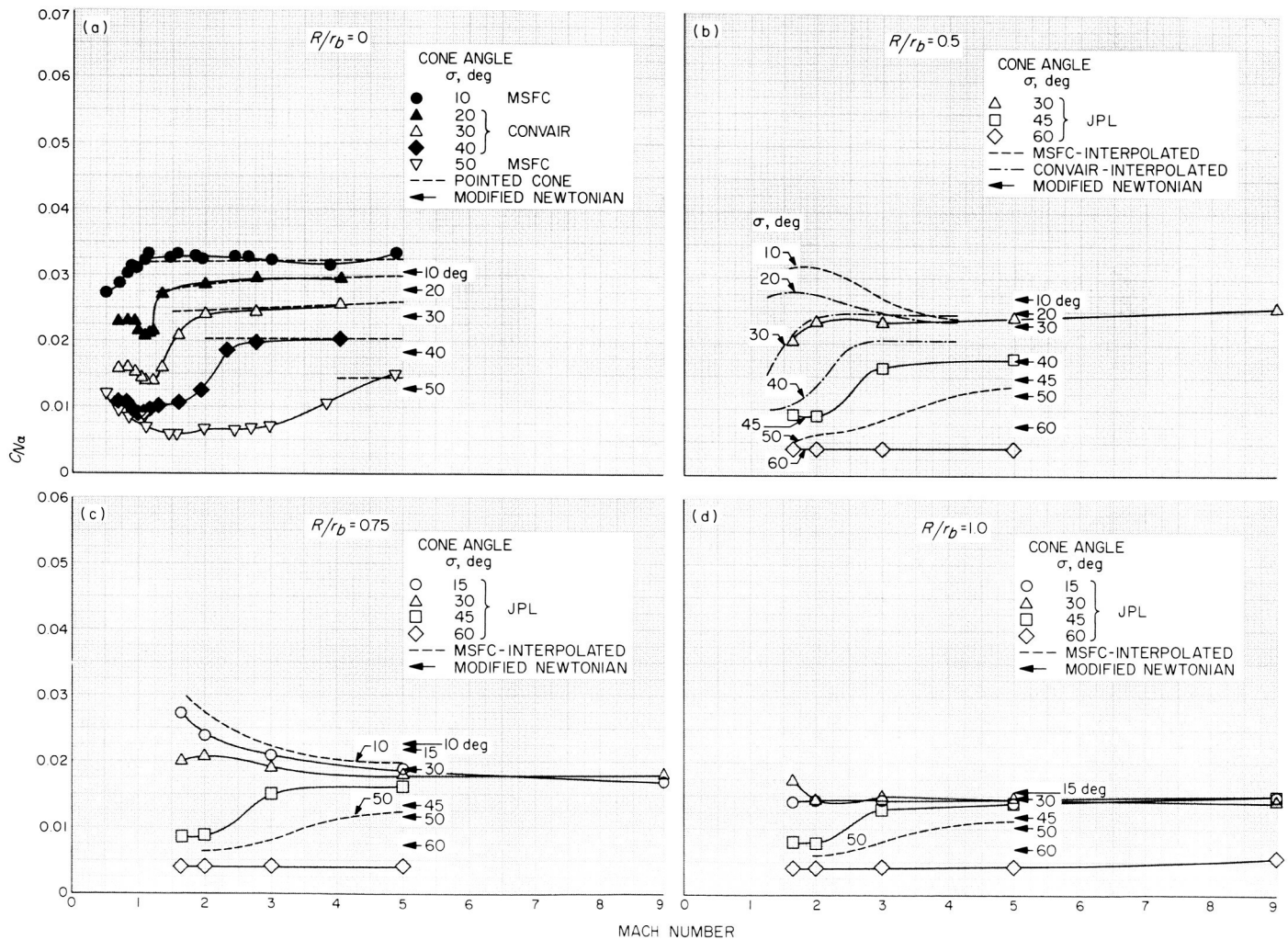


Fig. 4. Variation of normal force coefficient slope with Mach Number—spherically blunted cones: (a)  $C_{N\alpha}$  vs. Mach No.,  $R/r_b = 0$ ; (b)  $C_{N\alpha}$  vs. Mach No.,  $R/r_b = 0.5$ ; (c)  $C_{N\alpha}$  vs. Mach No.,  $R/r_b = 0.75$ ; (d)  $C_{N\alpha}$  vs. Mach No.,  $R/r_b = 1.0$



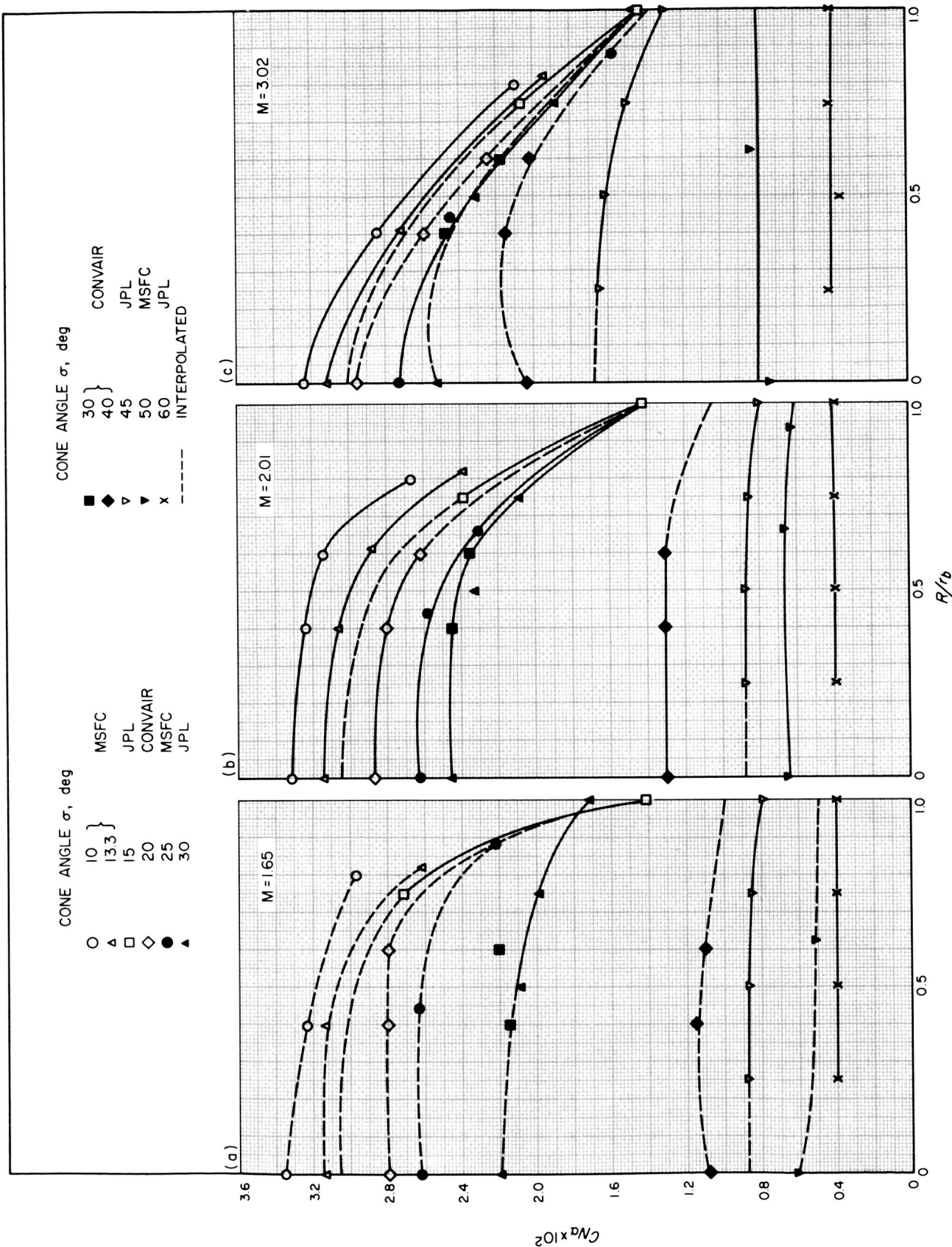


Fig. 5. Variation of normal force coefficient slope with bluntness—spherically blunted cones: (a)  $C_{N\alpha}$  vs.  $R/r_b$ ,  $M = 1.65$ ; (b)  $C_{N\alpha}$  vs.  $R/r_b$ ,  $M = 2.01$ ; (c)  $C_{N\alpha}$  vs.  $R/r_b$ ,  $M = 3.02$

## B. Center of Pressure at Zero Angle of Attack $X_{cp}/D$

The center of pressure is measured from the base of the model and is found to be practically independent of the tested angle of attack. Forward is taken as positive direction.

### 1. Round-Shouldered Cylinders

Center of pressure location versus Mach number is presented in Fig. 6a for various shoulder radius ratios. These data show that the center of pressure is aft of the base and moves forward as the shoulder radius becomes

larger. Except for the most blunt case,  $r_c/r_b = 0.25$ , there is little variation with Mach number. Modified Newtonian theory predicts a constant center of pressure location and is seen to be forward of experimental values.

A cross plot of the data, Fig. 6b, shows the variation of  $X_{cp}$  with shoulder radius ratio.

### 2. Spherical Segment Models

Figure 7a shows that the center of pressure location varies only slightly with Mach number and moves aft with increasing base angle, i.e., increasing bluntness. This is also

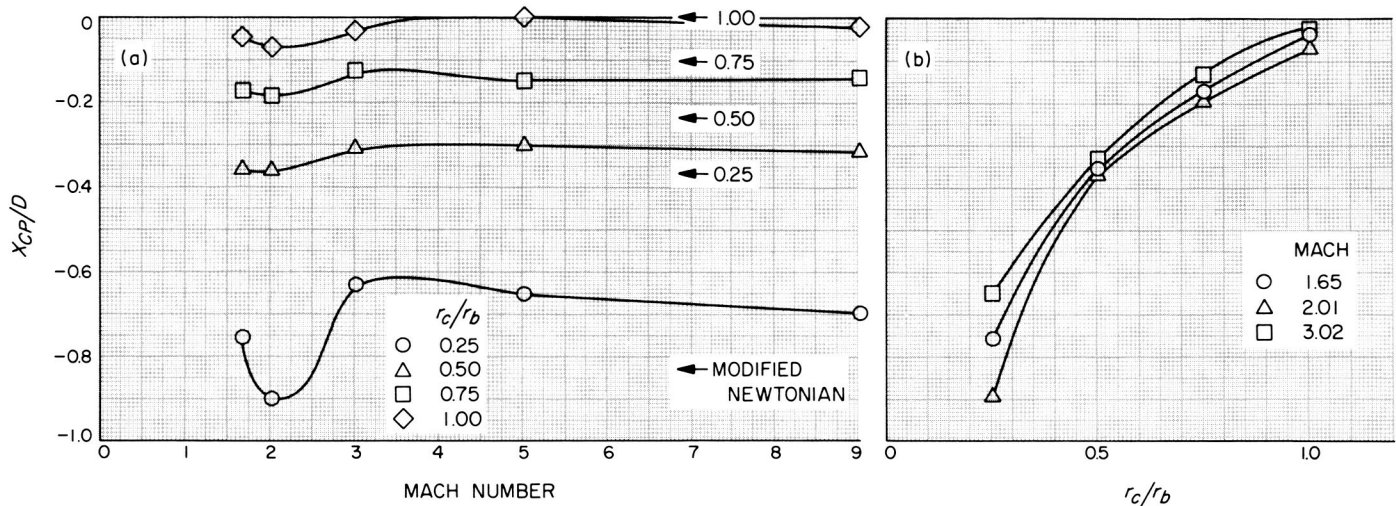


Fig. 6. Variation of center of pressure location—round-shouldered cylinders: (a)  $X_{cp}/D$  vs. Mach No.; (b)  $X_{cp}/D$  vs. shoulder radius ratio

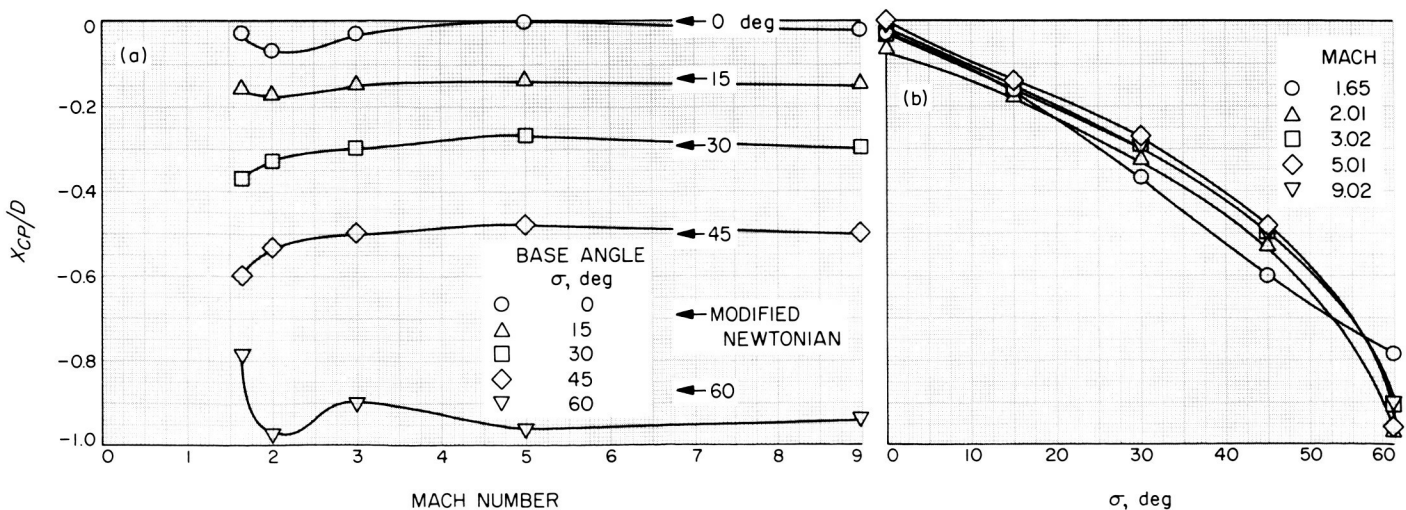


Fig. 7. Variation of center of pressure location—spherical segment models: (a)  $X_{cp}/D$  vs. Mach No.; (b)  $X_{cp}/D$  vs. base angle



shown in the cross plot Fig. 7b. Modified Newtonian theory quite accurately predicts the center of pressure for these models except for the 60-deg model.

### 3. Blunted Cones

Figure 8 shows the variation of center of pressure location with Mach number and cone half-angle for various bluntness ratios. The data for bluntness ratio  $R/r_b = 0$  shown in Fig. 8a are taken from Ref. 1 and 2. Except for

the bluntest case,  $R/r_b = 1.0$ , and base angle of 60 deg, modified Newtonian theory adequately predicts  $X_{cp}/D$  for  $M > 2.0$ .

Figure 9 is a cross plot of  $X_{cp}/D$  showing variation with bluntness ratio and cone half-angle. The data show that at low supersonic Mach numbers the cones are fairly insensitive to bluntness up to a bluntness of about  $R/r_b = 0.5$ . The effect of bluntness decreases with increasing cone half-angle.

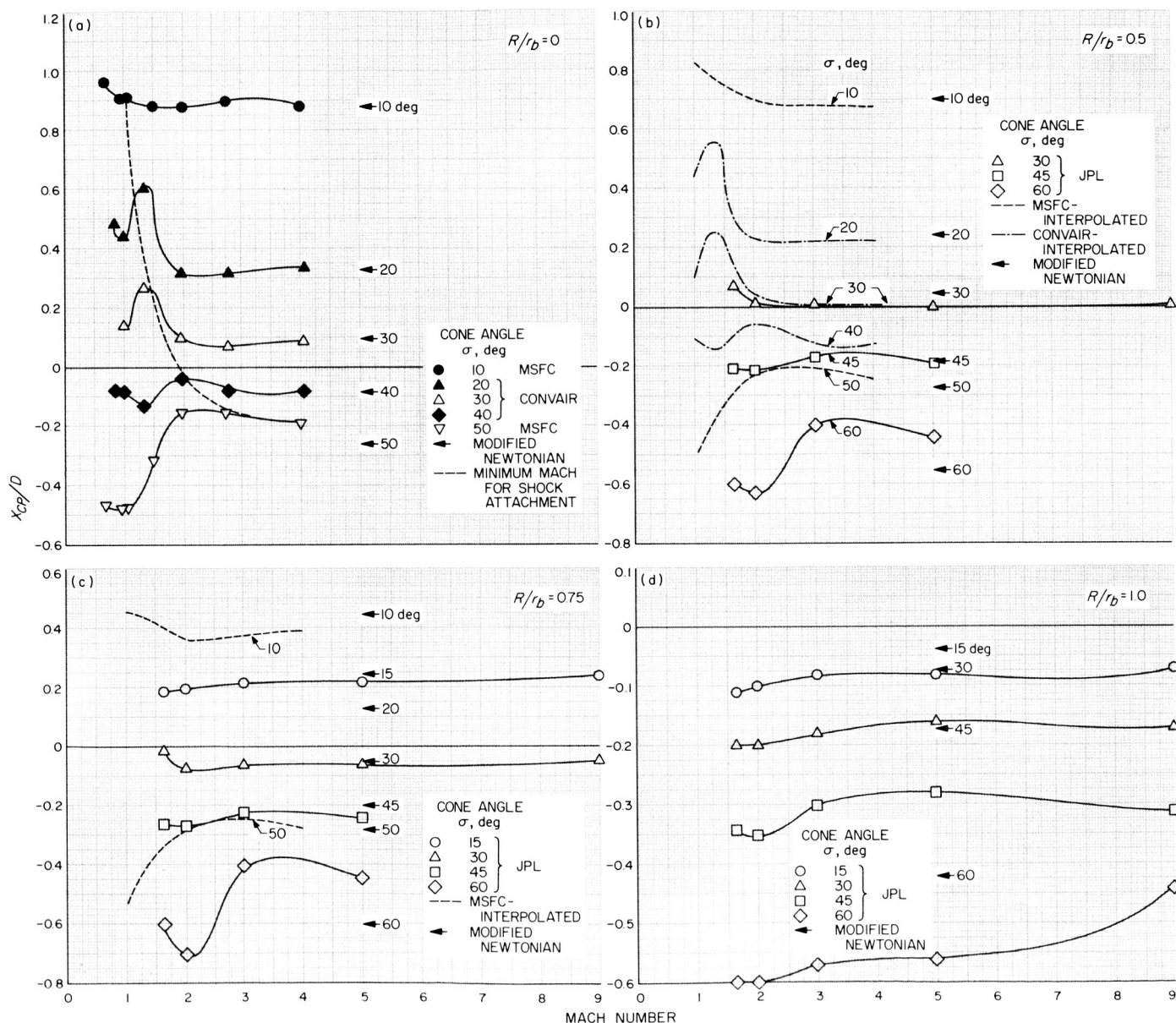


Fig. 8. Variation of center of pressure location at zero angle of attack—spherically blunted cones: (a)  $X_{cp}/D$  vs. Mach No.,  $R/r_b = 0$ ; (b)  $X_{cp}/D$  vs. Mach No.,  $R/r_b = 0.5$ ; (c)  $X_{cp}/D$  vs. Mach No.,  $R/r_b = 0.75$ ; (d)  $X_{cp}/D$  vs. Mach No.,  $R/r_b = 1.0$

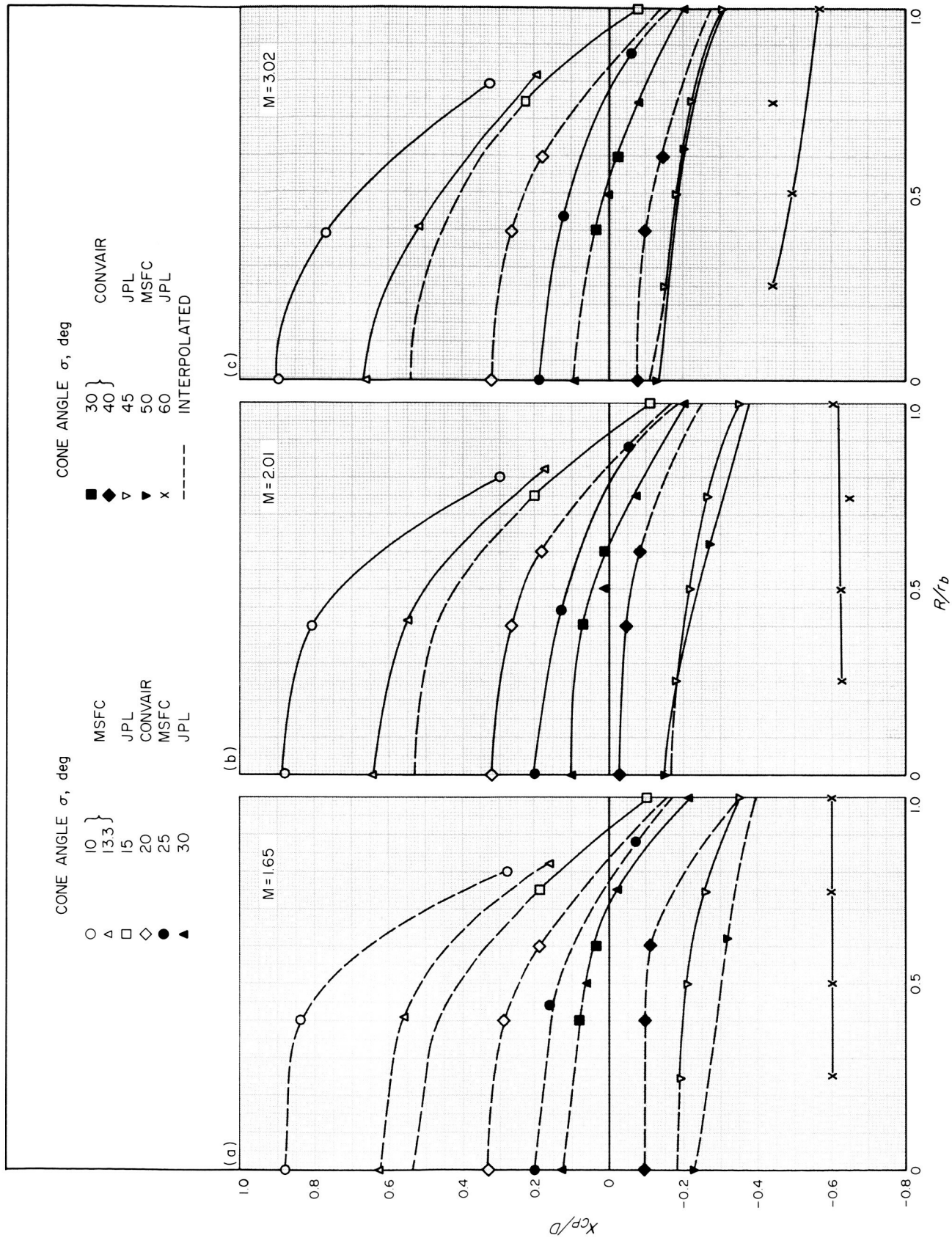


Fig. 9. Variation of center of pressure location with bluntness—spherically blunted cones: (a)  $X_{cp}/D$  vs.  $R/r_b$ ,  $M = 1.65$ ; (b)  $X_{cp}/D$  vs.  $R/r_b$ ,  $M = 2.01$ ; (c)  $X_{cp}/D$  vs.  $R/r_b$ ,  $M = 3.02$

### C. Axial Force Coefficient at Zero Angle of Attack $CA_{\alpha=0}$

The reference area for the force coefficients is the model base area. The forces were measured with a strain gage balance and when the data were reduced the base drag was subtracted so that the axial force coefficient presented represents the forebody drag only. At  $M = 1.65$ , 2.01, and 3.02 the base pressure was measured, but at  $M = 5.01$  and 9.02 the base pressure was assumed to be zero. This assumption causes the drag due to base pressure to be overestimated; therefore, the axial force coefficients presented are low at  $M = 5.01$  and 9.02. The error is estimated to be about 10% of the total drag for the lowest drag body at  $M = 5.01$  and about 3% at  $M = 9.02$ . The drag due to base pressure is shown in Fig. 10a and is applicable to all model configurations.

#### 1. Round-Shouldered Cylinders

Figures 10a and 10b present the axial force coefficient versus Mach number and axial force coefficient versus

shoulder radius ratio, respectively. The data for the disk were taken from Ref. 5 and data from Ref. 6 were used to extend the hemisphere data to subsonic Mach numbers. Modified Newtonian theory is quite accurate in predicting  $CA$  for the hemisphere  $r_c/r_b = 1.0$  but, as would be expected, overestimates the drag on the disk.

#### 2. Spherical Segment Models

Figures 11a and 11b present the axial force coefficient data for the spherical segment models. Here again, modified Newtonian theory is more accurate for these models than for the cylinders.

#### 3. Blunted Cones

Figure 12 presents the axial force coefficient versus Mach number for blunted cones of various bluntness ratios. As expected, increasing cone half-angle increases  $CA$ . For clarity modified Newtonian values are presented

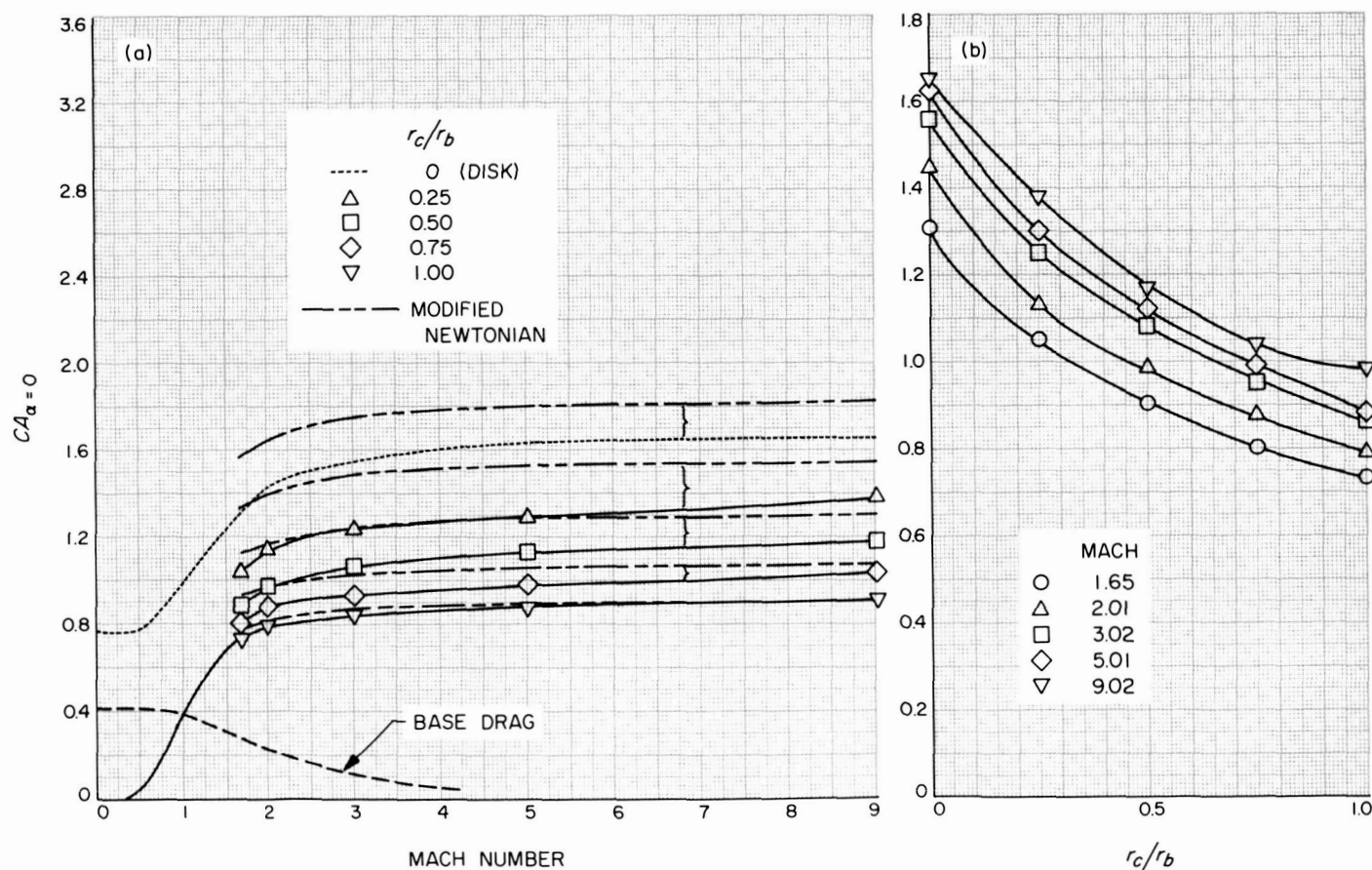


Fig. 10. Variation of axial force coefficient—round-shouldered cylinders: (a)  $CA_{\alpha=0}$  vs. Mach No.; (b)  $CA_{\alpha=0}$  vs. shoulder radius ratio

at  $M = 5.0$  only. Figure 13 is a cross plot showing the effect of bluntness and Fig. 14 shows the effect of cone half-angle. For small angle cones,  $CA$  increases with increasing bluntness; however, this effect decreases with

increasing cone angle and the effect of bluntness disappears for cones of about 40 deg of half-angle. Experimental values agree very well with sharp cone theory except for the 40-deg cone at  $M = 2.01$ .

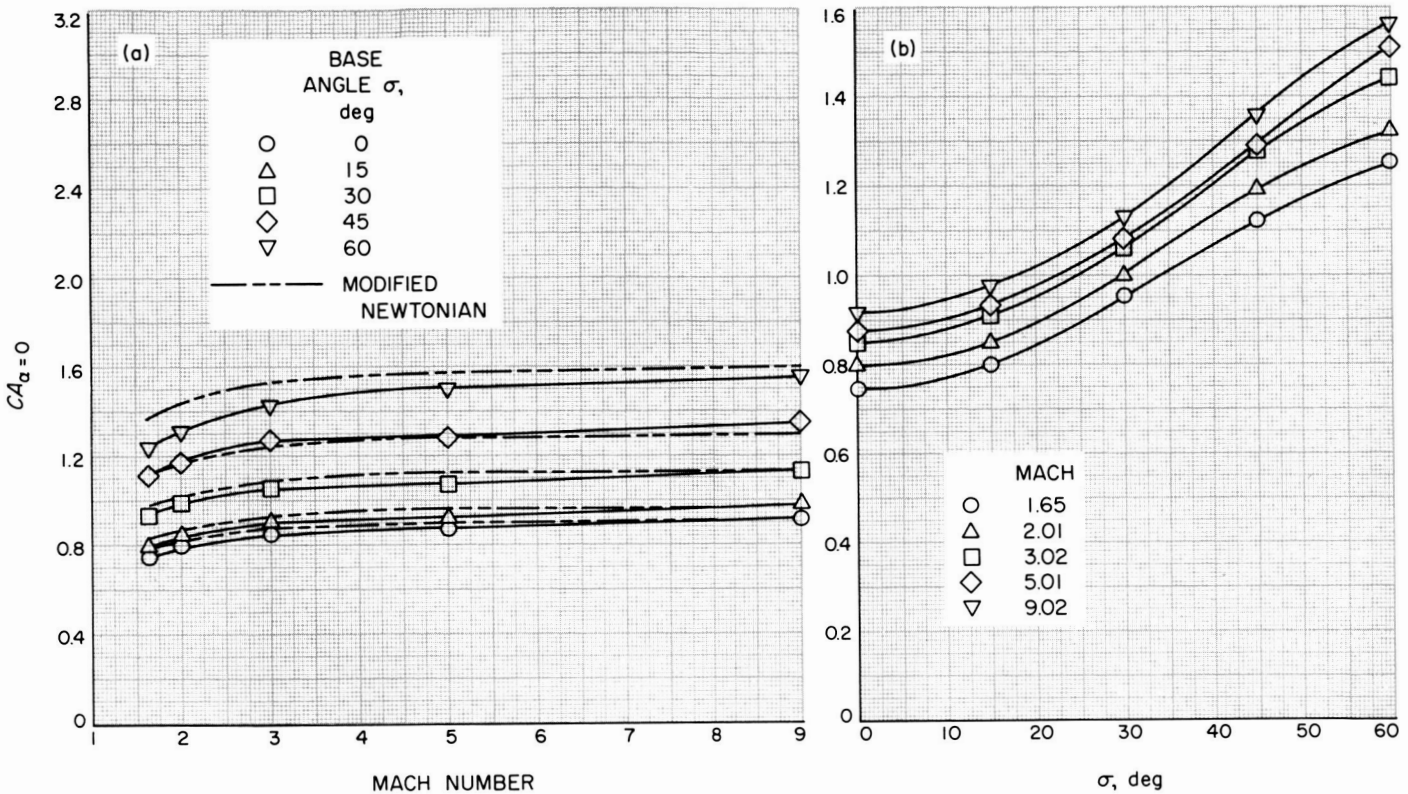


Fig. 11. Variation of axial force coefficient—spherical segment models: (a)  $CA_{\alpha=0}$  vs. Mach No.; (b)  $CA_{\alpha=0}$  vs. base angle



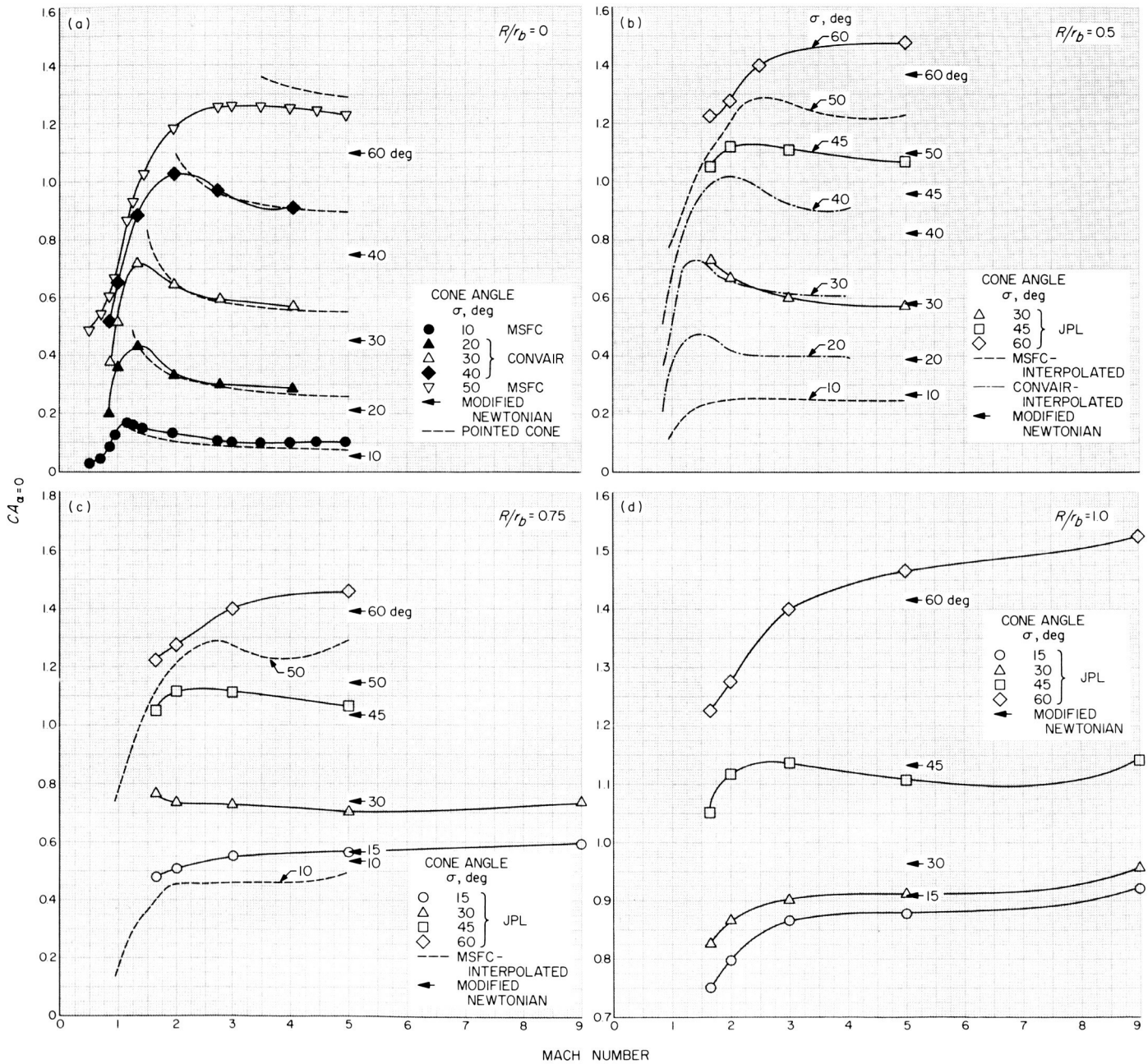


Fig. 12. Variation of axial force coefficient with Mach number—spherically blunted cones: (a)  $CA_{\alpha=0}$  vs. Mach No.,  $R/r_b = 0$ ; (b)  $CA_{\alpha=0}$  vs. Mach No.,  $R/r_b = 0.5$ ; (c)  $CA_{\alpha=0}$  vs. Mach No.,  $R/r_b = 0.75$ ; (d)  $CA_{\alpha=0}$  vs. Mach No.,  $R/r_b = 1.0$

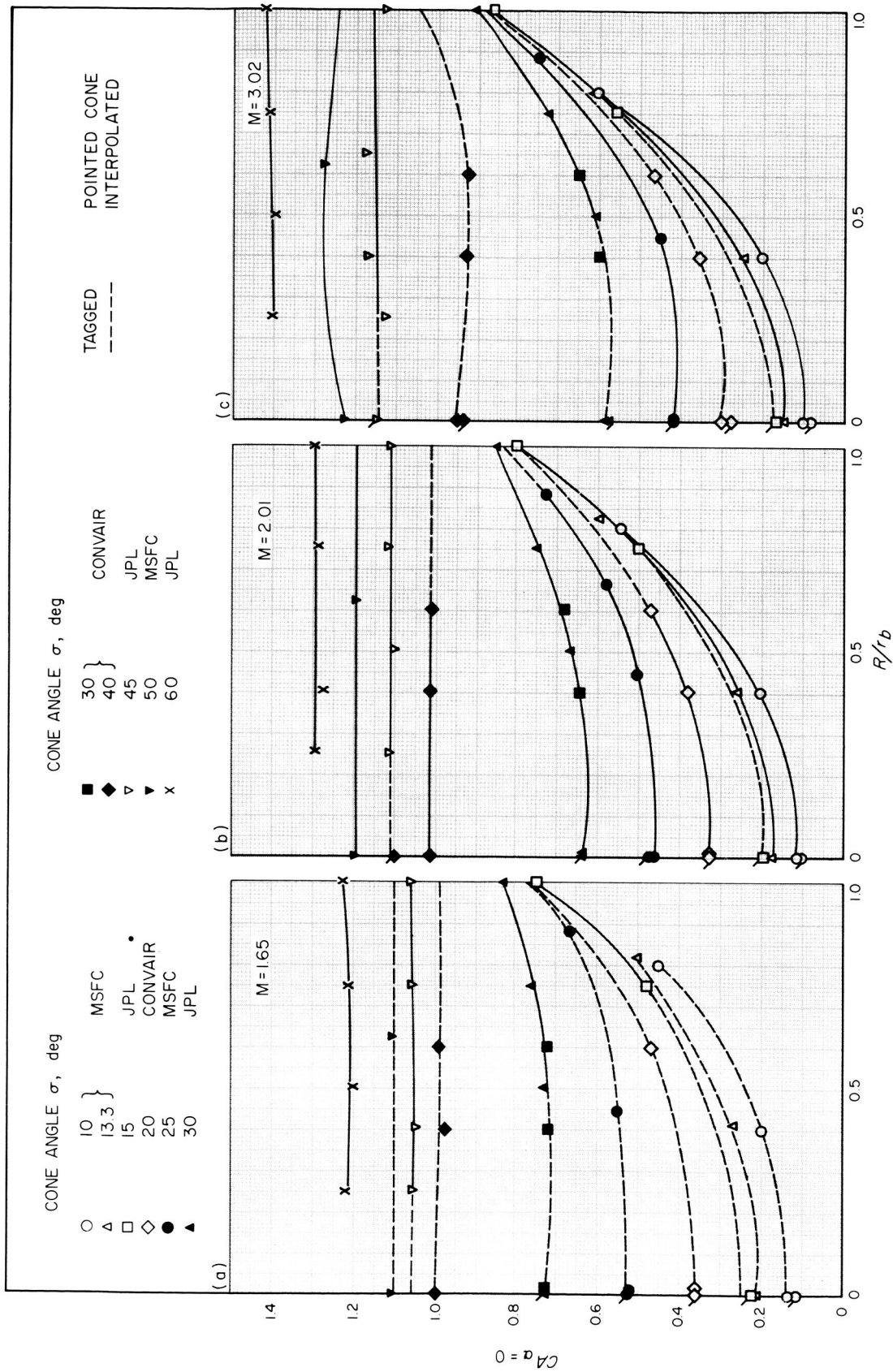


Fig. 13. Variation of axial force coefficient with bluntness—spherically blunted cones: (a)  $CA_{\alpha=0}$  vs.  $R/r_b$ ,  $M = 1.65$ ; (b)  $CA_{\alpha=0}$  vs.  $R/r_b$ ,  $M = 2.01$ ; (c)  $CA_{\alpha=0}$  vs.  $R/r_b$ ,  $M = 3.02$

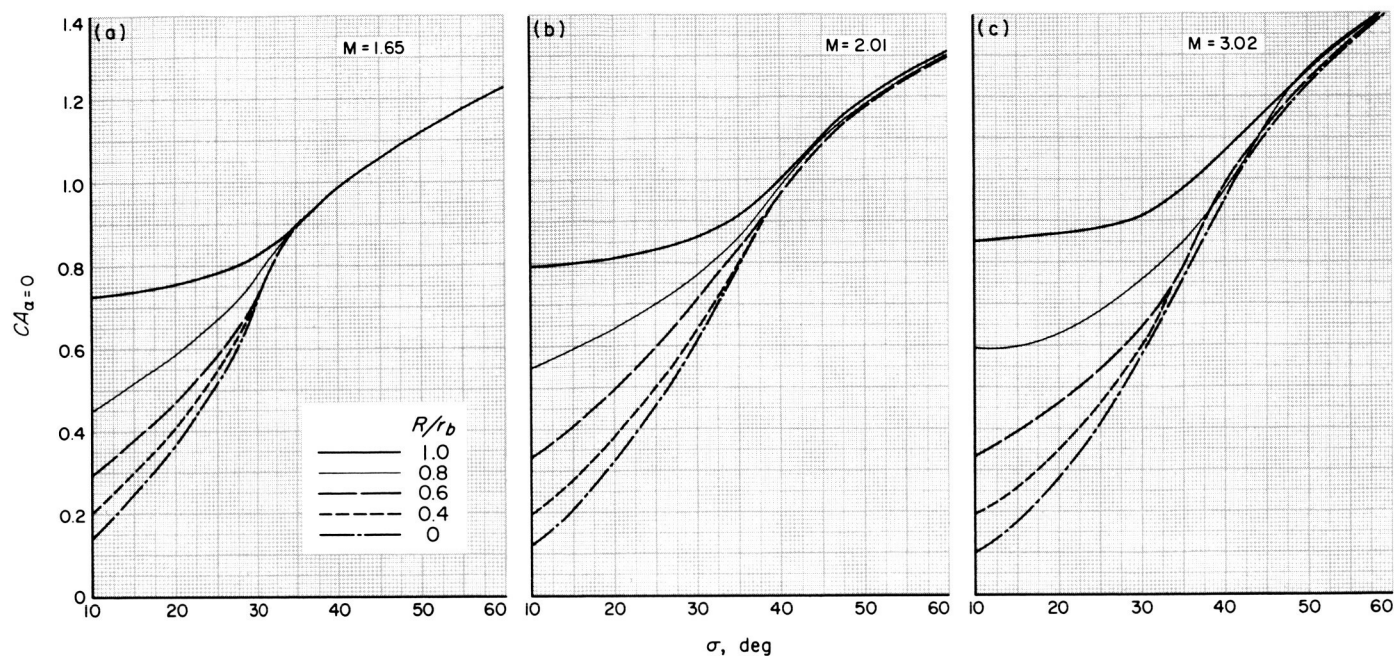


Fig. 14. Variation of axial force coefficient with cone half-angle—spherically blunted cones: (a)  $CA_{\alpha=0}$  vs.  $\sigma$ ,  $M = 1.65$ ; (b)  $CA_{\alpha=0}$  vs.  $\sigma$ ,  $M = 2.01$ ; (c)  $CA_{\alpha=0}$  vs.  $\sigma$ ,  $M = 3.02$

### III. CONCLUSIONS

1. The curve of  $C_N$  versus angle of attack is fairly linear over the test range of angle of attack for most of the test configurations; however, linearity decreases with increasing bluntness.
2. In general, the data for pointed cones agree well with pointed cone theory.
3. Modified Newtonian theory predicts the trend of the data for all models, but generally cannot be depended upon for absolute values.
4. The data obtained up to  $M = 9$  indicates that the data variation with Mach number above  $M = 3$  is generally slight.
5. For blunted cone models at low supersonic Mach numbers, bluntness has little effect on the data for bluntness ratios below 0.5.
6. Data for blunted cones with half-angles greater than 40 deg are practically unaffected by changes in bluntness ratio.
7. Except for the bluntest models, F-25 and 60-deg blunted cones, the center of pressure location varies only slightly with Mach number above  $M = 2$  and is practically independent of angle of attack over the range of the test.

### NOMENCLATURE

$A$	reference area, model base area
$CA_{\alpha=0}$	axial force coefficient, (axial force/ $qA$ ) — $CPB$
$C_{N\alpha}$	slope of normal force coefficient curve/deg
$CPB$	base drag coefficient, $(P - P_b)/q$
$D$	base diameter
$M$	Mach number
$P$	static pressure
$P_b$	base pressure
$q$	dynamic pressure, $\frac{1}{2}\rho V^2$
$R$	radius of spherical nose on blunted cone models
$r_b$	radius of model base
$r_c$	shoulder radius (Fig. 1a)
$r_c/r_b$	shoulder radius ratio, cylinder models
$R/r_b$	bluntness ratio, blunted cones
$X_{cp}$	center of pressure location measured from base, forward positive
$\sigma$	base angle of spherical segment models and cone half-angle for blunted cone models



## REFERENCES

1. Marshall Space Flight Center, *Aerodynamic Characteristics of Spherically Blunted Cones at Mach Numbers from 0.5 to 5.0*, MTP-AERO-61-38, Marshall Space Flight Center, Huntsville, May 2, 1961.
2. Geudtner, W. J., Jr., *Sharp and Blunted Cone Force Coefficients and Centers of Pressure from Wind Tunnel Tests at Mach Numbers from 0.50 to 4.06*, Report No. ZA-7-017, Convair, a Division of General Dynamics Corporation, San Diego, June 16, 1955.
3. Ames Research Staff, *Equations, Tables, and Charts for Compressible Flow*, NACA Report 1135, National Aeronautics and Space Administration, Washington, D. C., 1953.
4. Gray, Don J., *Drag and Stability Derivatives of Missile Components According to the Modified Newtonian Theory*, AEDC-TN-60-191, Arnold Engineering Development Center, Tullahoma, Tenn., November, 1960.
5. Hoerner, Sigward F., *Fluid-Dynamic Drag*, published by author, Midland Park, N. J., 1958, p. 15-16.
6. Koelle, Heinz Hermann, *Handbook of Astronautical Engineering*, McGraw-Hill Book Co., Inc., New York, 1961, p. 5-24.